Aerosol and Air Quality Research, 17: 69–83, 2017

ISSN: 1680-8584 print / 2071-1409 online
doi: 10.4209/aaqr.2016.05.0216

Effects of Polluted Air-Masses Advection on Atmospheric Particles in a Semi-Rural Site in South Italy by SEM-EDX Analysis

Antonio Lettino[1], Mariarosaria Calvello[1*], Francesco Esposito[2], Saverio Fiore[1], Marina Lorusso[1], Giulia Pavese[1]

[1] *Consiglio Nazionale delle Ricerche- Istituto di Metodologie per l'Analisi Ambientale (CNR-IMAA), 85050 Potenza, Italy*
[2] *Università della Basilicata - Scuola di Ingegneria, C.da Macchia Romana, 85100 Potenza, Italy*

ABSTRACT

The variation of aerosol properties under polluted air masses advection was studied in a semi-rural site in South Italy, by means of SEM-EDX analysis performed on particles collected on 13-stages impactor filters. Radiometric measurements, HYSPLIT back-trajectories and NAAPS maps helped to choose four measurement days of polluted air mass circulation, two of them collected in the warm season (31 July 2008, 16 September 2010) and two in the cold one (16 April 2009, 18 March 2010). Polluted aerosol characteristics were compared to those under background (BG) conditions (8 February 2011), highlighting differences in the particles chemical and morphological properties. One of the signatures of the air mass transport in the coarse fraction was the higher content of particles containing S, i.e., S-reacted, (27.5% on average) in comparison with BG conditions (1%). Two main sources of transported aerosols were identified: industrial processes and biomass burning, with fly ash, metal and S-rich particles in the first case, and K-salts and nitrate-coated Ca-bearing-particles in the second. Single particle analysis on the coarse fraction allowed large agglomerates of soot to be identified, with inclusions of silicate particles rich in Cu and Zn, Ca-S, fly ash and metals particles that are a clear indication of extensive modifications of aerosol size, chemical composition and, likely, radiative properties. In finer stages (EAD $\leq$ 0.94 μm) concurrent collection of organic and inorganic particles originated an agglomerate state matter mainly characterized by K and S for polluted conditions and by K only for BG.

Keywords: Atmospheric aerosol; Long-range transport; Air pollution.

INTRODUCTION

The importance of aerosols impact on the climate is well established, even if large uncertainties still remain on the amplitude of these effects (IPCC, 2013) due to the concurrent processes of scattering (negative radiative forcing) and absorbing solar radiation (positive radiative forcing) by different aerosol types and to their influence on cloud formation. For a proper estimation of aerosol contribution to the radiative forcing, uncertainties in radiative transfer models need to be reduced. Aerosols also play a crucial role from the perspective of adverse consequences on human health (Janssen *et al.*, 2011). All the above- mentioned effects depend on aerosols physico-chemical properties and on their mixing state/processes. In the case of black carbon, for example, its absorption properties can be modified if a coating with non-absorbent material is present (Moffet *et al.*, 2013) or if some mixing effect occurred (Cheng *et al.*, 2015). As it concerns impact on health, Molina *et al.* (2013) found that geochemical alteration of Zn- particles during weathering can strongly impact the bioavailability of Zn.

In general, metal particles internally mixed with sulfates, after inhalation, will deposit deeper into the respiratory system or, more generally water-soluble matter will leave trace elements in many parts of the human body, penetrating cell membranes and producing worst effects than free-floating metal particles (Adachi *et al.*, 2010; Pardo *et al.*, 2016).

Aerosols mixing and transformation processes are of great importance especially in the case of transport episodes characterized by a high probability of interaction among particles and by the abundance of aged aerosols. Transport phenomena can thus strongly influence and modify local aerosol properties with repercussions on a wider scale. For example, SO_2-rich air masses can reduce, through acidification, the nucleating properties of ice nuclei in the Arctic region (Jouan *et al.*, 2014) demonstrating that impact of long-range transport is fundamental, not only for urban polluted sites, but also for remote and rural site, where aerosols carried by air circulation can represent the main source of pollution. In particular, the Mediterranean basin is frequently influenced by air masses coming from North-

* Corresponding author.
E-mail address: mariarosaria.calvello@imaa.cnr.it

Eastern Europe, where obsolete industrial plants, coal power plants (Bovchaliuk *et al.*, 2013) and relevant biomass burning (Diapouli *et al.*, 2014; Popovicheva *et al.*, 2014) represent an important pollution source.

The main goal of this study is to understand how polluted air masses, with long-range transport of particles, influence aerosol composition in a semi-rural site of the Mediterranean basin and how aging influences physical, chemical and mineralogical properties of aerosol. A previous study conducted in this area by Caggiano *et al.* (2011) on $PM_{2.5}$ during the period 26 June 2006–11 July 2006 highlighted the occurrence of trans-boundary advection phenomena. In present study additional information on aerosol transformation and aging effect were obtained by means of a SEM-EDX detailed morphological analysis. SEM observations combined with EDX technique are recognized as a powerful tool to obtain in depth information on speciation, aggregation and coating of different aerosol types thus revealing the influence of mixing, aging and secondary particle formation processes (Lettino *et al.*, 2013; Geng *et al.*, 2014; Li *et al.*, 2016). To this aim SEM-EDX analysis was carried out on aerosol particles collected by a 13-stage impactor at a semi-rural site in South Italy affected by four episodes of polluted air mass advection from northeastern Europe, in different periods of the year, and the results were compared with measurements under BG conditions.

METHODS

Site Description

Measurements were performed in South Italy (40.60°N, 15.72°E, 750 m a.s.l.) at the semi-rural site of Tito Scalo, where the Methodologies for the Environmental Analysis Institute is located (Fig. 1). Despite its latitude, a continental climate and cold winters characterize this site, due to the influence of the surrounding Apennines. Based on monthly mean temperatures, two main seasons can be identified: the cold one from November to April with temperature values ranging between 3.8–8.5°C and the warm one from May to October with temperature values ranging between 14.1–23.4°C (http://cma.entecra.it/atlante/19_tabelle.pdf). These temperature values were estimated over the years 1981–2010.

Stoves for heating of private houses contribute to carbonaceous aerosol production in winter time, whereas a freeway about 1 km far from the Institute is a source of both carbonaceous and re-suspended particles throughout the year. Agricultural activities at a local scale can influence aerosol composition in different ways, depending on the season. In particular, waste burning of olive tree branches can contribute to aerosol production in winter/spring periods, whereas wheat straw burning can be present during summer. A few small factories such as a steel plant located about

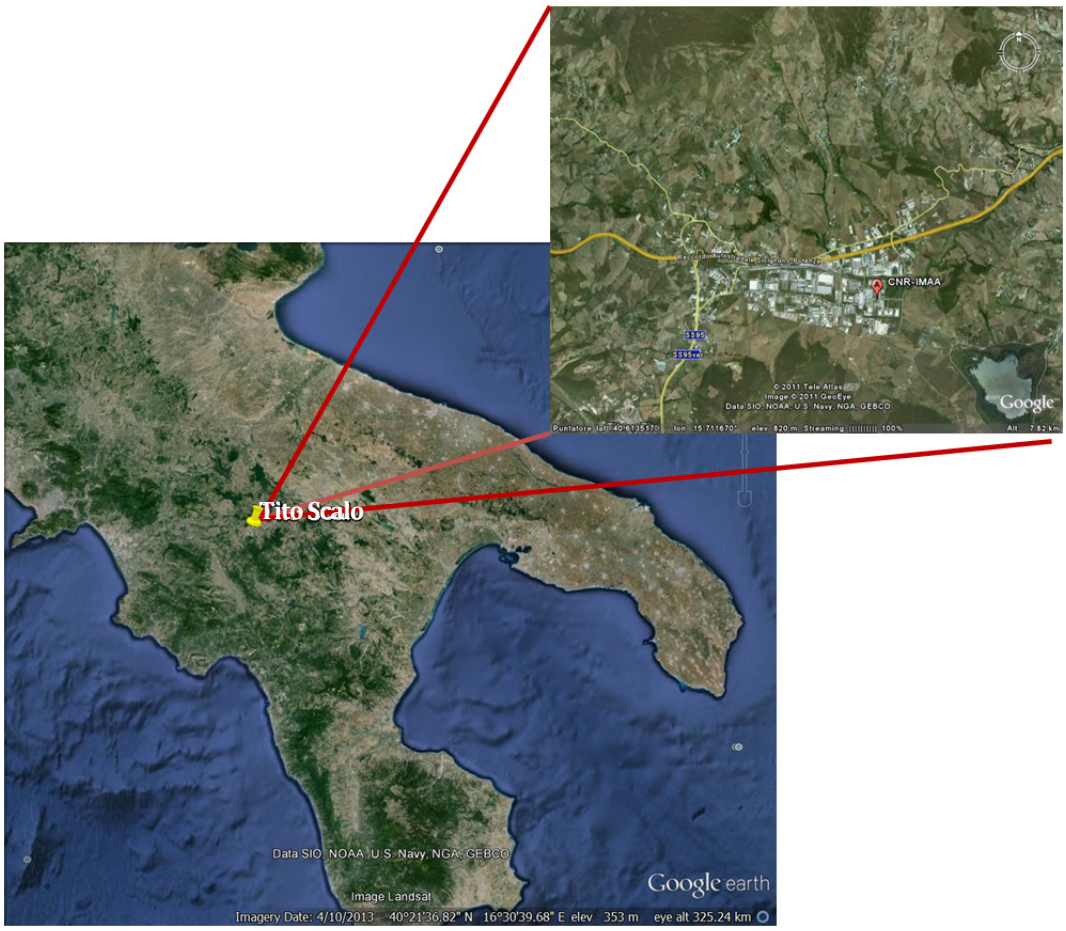

Fig. 1. Location of the measurements site in South Italy as obtained by Google Earth.

10 km from the site contribute to local emissions. As verified in Calvello *et al.* (2010), HYSPLIT back-trajectories (Draxler and Rolph, 2003) generated for the site reveal prevailing aerosol transport paths from north-eastern Europe, north Africa or from the Atlantic Ocean. Therefore, depending on the atmospheric circulation, anthropogenic, sea-salt and mineral dust particles can reach the measurement site, highlighting aging effects due to long-range transport.

Instruments and SEM-EDX Technique

Atmospheric aerosols were collected at the ground by means of a 13 stage Dekati Low Pressure Impactor (DLPI hereafter), allowing for the measurement of aerosol mass size distributions. The instrument inlet was placed at about 2 m above the ground with a sampling time of 24 hours. The DLPI, equipped with polycarbonate filters, covers the size range 0.03 μm–10.0 μm with a sampling flow rate of 30 L min^{-1} and with 50% stage cut off Equivalent Aerodynamic Diameters (EAD). In Table 1 the EADs dimensions corresponding to the 13 stages are reported. A detailed description of the measurement procedure is reported in Calvello *et al.* (2010). Particulate set down on DLPI filters was analyzed by means of a field emission scanning electron microscope (FESEM, Zeiss Supra 40) coupled with an energy-dispersive X-ray spectrometer (EDS, Oxford Inca Energy 350). This configuration allowed for the characterization of particles as small as few tens of nanometres, recording high resolution images from an in-lens secondary electron detector. A small portion (0.5 cm^2) of the filters was attached to an aluminum stub (12 mm in diameter) using a carbon sticky tab and then carbon coated. The samples were studied using images taken by secondary electron (SE) and back-scattered electron (BSE) detectors. The EDS system can detect elements with an atomic number $Z > 4$, since it is equipped with an energy dispersive Si(Li) detector with an ultra-thin window (INCA SATW). However, only elements with $Z > 10$ (Na) were considered in the X-ray spectra evaluation due to the samples carbon-coating and to the presence of carbon and oxygen in the polycarbonate filters. X-ray spectra were acquired at a 15 kV accelerating voltage using a 30 mm aperture size.

SEM analysis of particulate was performed on impactor filters and, for each sampling, particles were grouped in fine (0.01 μm–0.94 μm, stages 1–8) and coarse (0.94 μm–9.77 μm, stages 9–13) fractions. Due to the sampling effects on finer stages (Wittmaack *et al.*, 2002) that favor the formation of an agglomerate state matter, the single particle analysis cannot be performed and only qualitative and indirect compositional information can be derived.

Conversely, quantitative analysis was performed on the coarse fraction by counting 350 particles per day, allowing the detection and the study of particles modified by the long-range transport.

A multi-year dataset of radiometric measurements of aerosol optical parameters over the column was analyzed in order to identify the advection of polluted air-masses over the measurement site. An Ocean Optics S2000 radiometer (spectral range 400 nm–800 nm, spectral resolution 1.5 nm), measuring direct solar irradiance with a time resolution of 15 minutes, allowed the estimate of aerosol optical depths (AOD) and Ångström parameters alpha and beta characterizing different aerosol loadings. These measurements were simultaneously collected with impactor samplings.

Table 1. DEKATI Impactor EAD particle ranges.

Stage	EAD particles range [μm]
1	0.01 ÷ 0.03
2	0.03 ÷ 0.06
3	0.06 ÷ 0.10
4	0.10 ÷ 0.16
5	0.16 ÷ 0.26
6	0.26 ÷ 0.38
7	0.38 ÷ 0.61
8	0.61 ÷ 0.94
9	0.94 ÷ 1.58
10	1.58 ÷ 2.35
11	2.35 ÷ 3.93
12	3.93 ÷ 6.47
13	6.47 ÷ 9.77

Sampling Days Selection

A data-set of 40 days corresponding to 986 ground-based radiometric measurements (AOD and Ångström parameters) collected during 2008, 2009, 2010 and 2011 along with air mass back-trajectories and NAAPS maps, were analyzed. The radiometric measurements procedure and data elaboration are described in detail in Esposito *et al.* (2004). The entire dataset is characterized by <AOD@780> = 0.18 ± 0.11 and <alpha> = 1.06 ± 0.60. According to the values of aerosol parameters and to the air mass paths, four days (31 July 2008, 16 April 2009, 18 March 2010, 16 September 2010) were selected for polluted conditions and one day (8 February 2011) for BG conditions. Higher values of AOD and alpha parameter generally characterize anthropogenic particles advection, suggesting, in comparison with clean data, an increased content of small particles. Such conditions were verified to influence the site for about 30% of measurements with air masses mainly coming from north-eastern Europe and in minor amount from north-central Europe. The scatter plot alpha vs. AOD@780 is shown in Fig. 2(a) for both polluted and BG days. Data corresponding to advected fine particles cover an area defined by $0.04 \leq AOD@780 \leq 0.48$ and $0.53 \leq alpha \leq 2.99$, whereas low aerosol loading correspond to $0.03 \leq AOD@780 \leq 0.12$ and $0.12 \leq alpha \leq 1.92$. As shown in Fig. 2(a), polluted points do not overlap with BG points. Moreover, as shown in Fig. 2(b), the frequency plot of alpha parameter shows 32% of polluted data greater than 1.6, against 12% of "clean" data. The advection of anthropogenic particles was confirmed by the Hysplit-generated air mass paths, calculated every 4 hours for each measurement day and found quite constant during the whole sampling period. As an example in Fig. 3, 5-days back trajectories at 12.00 a. m. corresponding to the days identified as both polluted and BG are reported, with ending points at 500 m, 1000 m, 1500 m a.g.l. Polluted paths originated in north-eastern Europe, except on 18 March 2010, when the crossed area was mainly north central Europe. In the case of BG, they

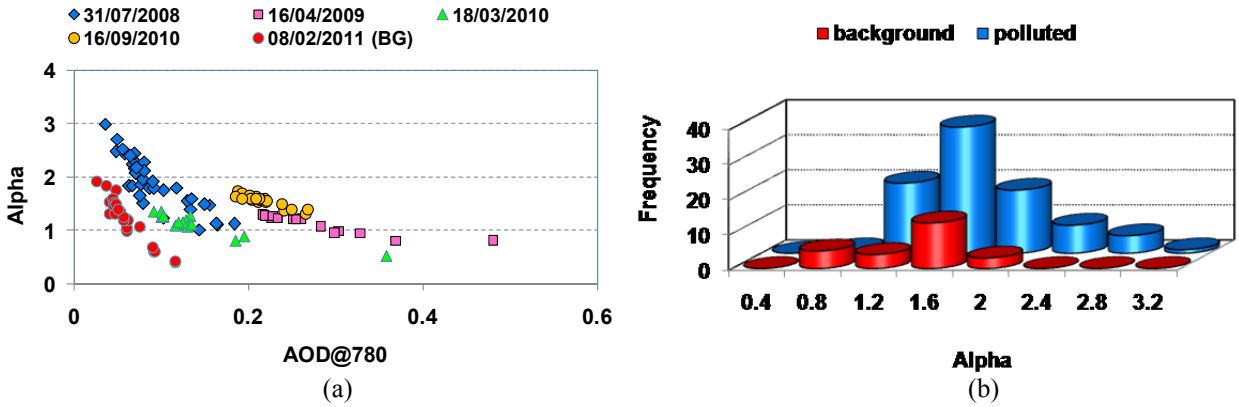

(a) (b)

Fig. 2. a): scatter plot of alpha parameter vs. AOD@780 for polluted days together with a BG day; b) frequency plot of alpha parameter for both polluted and BG data. Data were obtained every 15 minutes.

came from Atlantic Ocean and crossed western Europe. The NAAPS maps (available at the site http://www.nrlmry.navy.mil/aerosol) with different sulfates and smokes concentrations corresponding to the sampling days are shown in Fig. 4, where varying contributions from biomass burning smokes can be inferred.

RESULTS

SEM observations of aerosols collected on 13 filters of an impactor represented a powerful instrument to characterize the four polluted air masses. In Fig. 5 the corresponding four mass distributions and the BG distribution are shown. A preliminary analysis was performed on coarse filters revealing a homogeneity among particles. Then, direct and quantitative information on morphology and chemical composition of particulate was determined by means of single-particle analysis on stage 10 (1.58 μm ≤ EAD ≤ 2.35 μm), corresponding to the maximum of the coarse mode mass size distribution for all samplings except for 18 March. In this case the maximum occurred on stage 12 (3.93 μm–6.47 μm), where additional observations confirmed the general homogeneity among particles and therefore stage 10 was still considered representative for the analysis.

On the contrary, as said before, the fine fraction (particles with EAD < 1 μm) is constituted of an agglomerate state matter that allows to infer qualitative and indirect information only on the aerosol composition.

Single Particle Analysis on Coarse Fraction

Based on both morphology and chemical composition, coarse particles were classified into 9 different groups and compared with the BG composition, as reported in Table 2, where particle number percentages represent relative abundances of silicates and silicates with S, Ca-bearing particles, metal oxides and hydroxides, S-rich particles, soot, biogenic, Si-rich particles, fly ash, silicates mixtures and Silicate/S-rich mixtures. Silicates (with and without S), mostly constituted by Si and Al with Mg, K, Ca, Fe, Na, represented percentages varying from 15.6% to 53.8% of total particles. Provided that Saharan dust advection was excluded by radiometric data, impactor size distributions and HYSPLIT back trajectories, their high content can be partly attributed to the semi-rural environment of the site. Silicates with S are likely produced by combustion processes, or more generally by secondary reactions with S components present in the atmosphere to form sulfate-coated silicate particles (Li and Shao, 2009a; Tobo *et al.*, 2010). It is worth noting that the coating on silicates is responsible for a change in their hygroscopic properties enhancing their scattering efficiency and CCN (cloud condensation nuclei) activity (Li and Shao, 2009a). Contrary to BG conditions, polluted samplings always revealed the presence of silicates with S (Table 2).

Detailed silicates composition is shown in Table 3. Different kinds of aluminosilicates were found as, for example, clay minerals (Fig. 6(a)) with percentages varying from 12.3% to 51% of total silicates, and feldspars in minor amount (from 1.2% to 10%). Zn associated with Mg and Na aluminosilicates particles, was frequently detected by X-ray microanalysis spectra, highlighting both the presence of Zn species in the atmosphere and the significant role of clay minerals in metals transport (Hochella *et al.*, 2005).

Ca-bearing particles, present with the highest content in BG conditions, as shown in Table 4, were represented mostly by Ca-only and Ca-Mg particles (Fig. 6(b)). On 8 February 2011, 18 March 2010 and 31 July 2008 these particles were frequently found with a rounded and beam-damaged soluble-phase surface, suggesting a nitrate coating (Wittmaack *et al.*, 2002).

Metal particles included several classes, as described in Table 5 where Fe-particles represent the most common class, sometimes associated with Zn and in minor cases with Cu, Mn, Ti, S and Al. Metal particles showed a spherical morphology and a rough surface (Fig. 6(c)) in some cases, and in others were irregularly shaped and beam-damaged, indicating soluble metal species. Their percentages are comparable on polluted and BG samples.

Based on their chemical composition, different classes were identified within the S-rich particles group (Table 6). Ca-S were the most common particles, found as a hexagonal plate or an elongated shape (gypsum) in the greatest amount on 16 September 2010 (Fig. 6(d), left side). Sometimes they showed a soluble-phase surface, likely

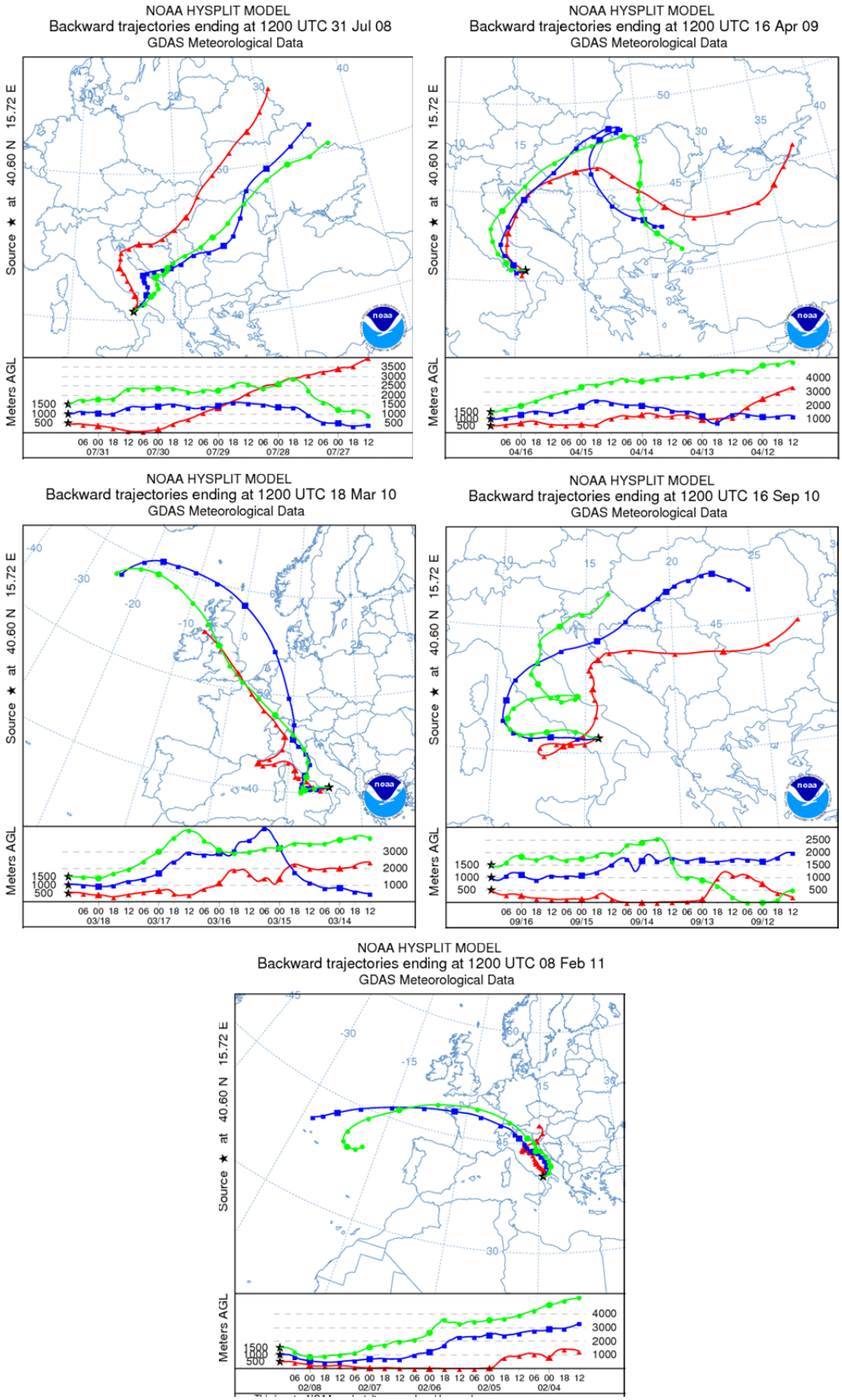

Fig. 3. HYSPLIT Air masses back-trajectories corresponding to the four polluted days and the BG day at 12:00 for 500, 1000, 1500 m a.g.l.

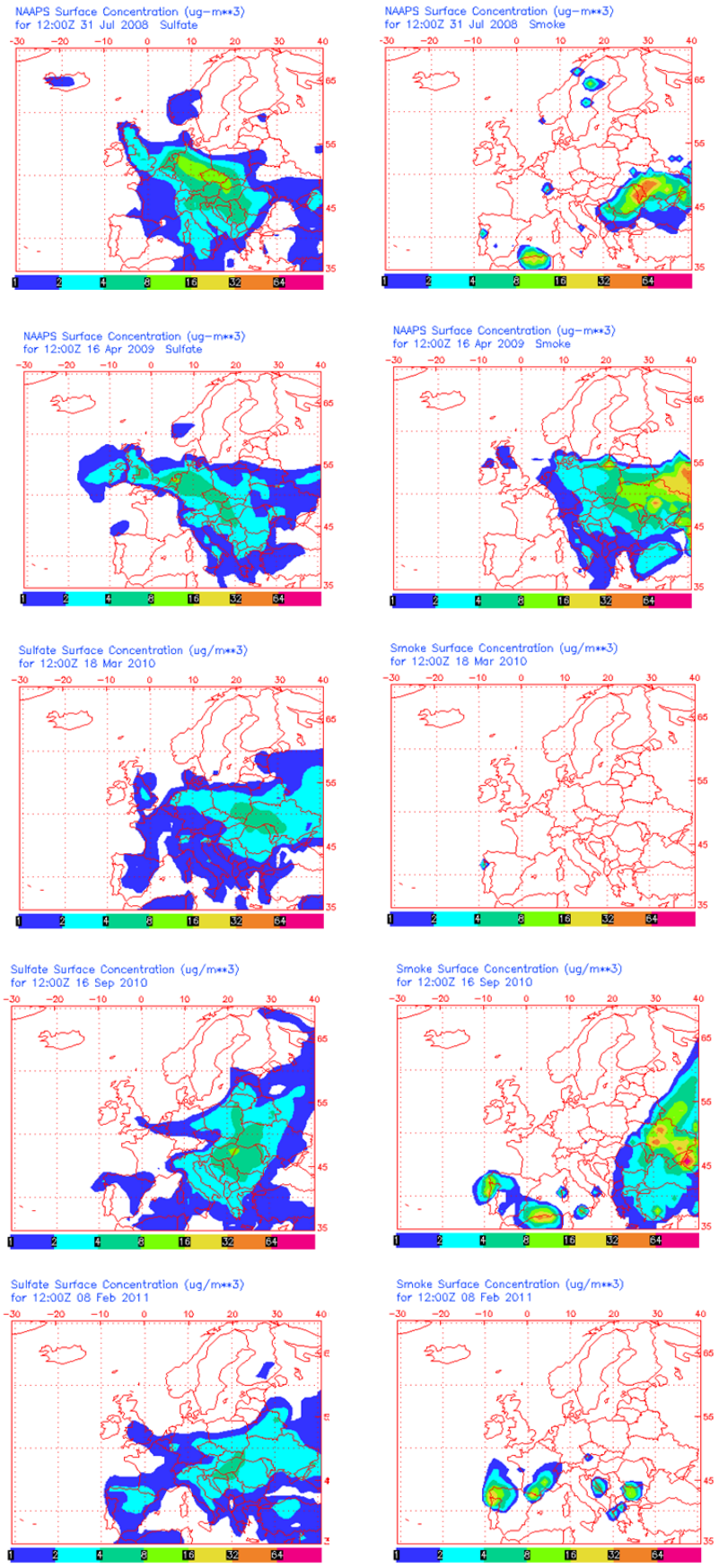

Fig. 4. NAAPS maps (sulfates and smokes concentrations) corresponding to the four polluted days and the BG day at 12:00.

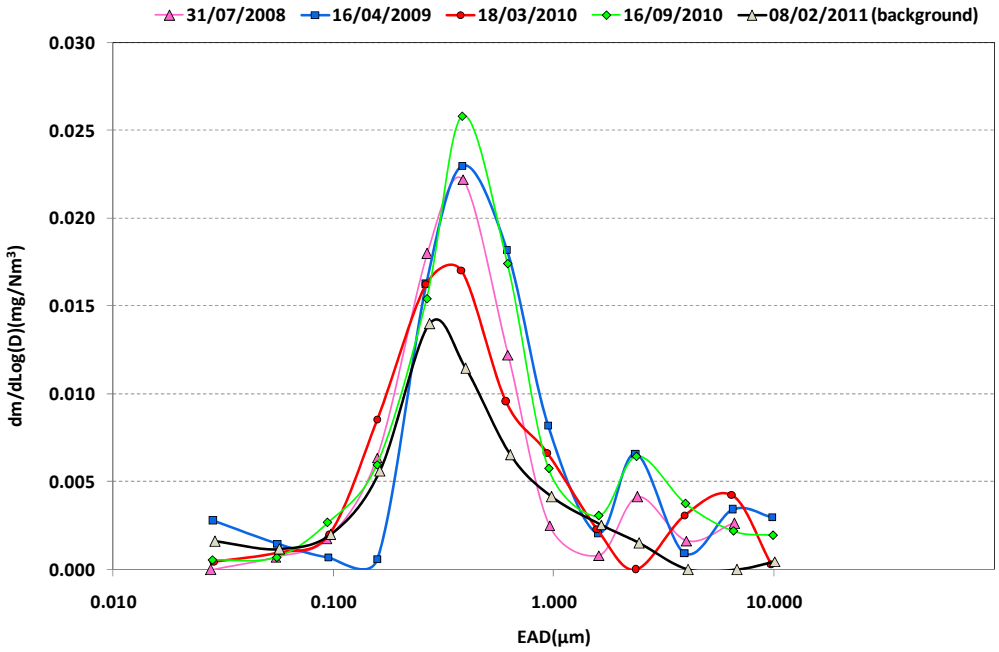

Fig. 5. Mass size distributions corresponding to one BG and four polluted days.

signifying a nitrate coating (Li and Shao, 2009a) (Fig. 6(d), right side). In addition, particles with a higher Ca to S ratio (Ca-rich-sulfate particle), if compared to Ca-S, were detected. These particles could represent the product of the incomplete transformation of carbonate particles (calcite and dolomite) into Ca-S particles. S-rich particles are quite rare on BG sample.

Soot showed complex chain-like structures consisting of linked spherules. In the BG sample, the soot particles number was higher than in polluted samples (Table 2), where chain-like structures more frequently formed large aggregates. Often these aggregates were internally mixed with primary phases (silicate particles, fly ash, Ca-bearing and metal particles) and secondary S-rich phases (Fig. 6(e), top panel) where the internal mixing is intended as particles inclusions in soot agglomerates, as in Li and Shao (2009b). Some primary silicates particles mixed with soot were characterized by Zn, Fe and Cu content.

In addition, tar balls (TB), found as isolated particles, were identified by their typical spherical or sub-rounded morphology, by their dimension (~200 nm) and by their stability under the electron beam (Posfai *et al.*, 2004). The dominant C element was sometimes accompanied by Si, Cl, K and S. Despite their typical dimension, TB were found in both BG and polluted coarse filters (Fig. 6(e), bottom panel), likely due to the sampling of larger water droplets containing them (Pavese *et al.*, 2016).

A rich group of biogenic particles was found in the warmer samples (10.5% on 31 July and 14.3% on 16 September) mainly made of pollens, spores and biogenic fragments (Fig. 6(f)). Peculiar morphology and elemental composition, made up mainly of C and O with minor P, K, Cl, and S characterized this group.

Si-rich particles (Si > 85%) were ubiquitous in all samples investigated with an average percentage concentration ranging from about 2.1 to the maximum of 8% found in BG conditions. Often Si-rich particles showed a rounded morphology differently from typical quartz shape (Popovicheva *et al.*, 2015) and, rarely, were observed as cenospheres, as in Fig. 6(g).

Fly ash are spherical particles with a size of about 2 µm (Fig. 6(h)) mainly composed of Si, Al, K, Fe, S, sometimes associated with Mg, Na, Ca. They were mostly found as isolated particles or included in soot agglomerates and their contribution to the total particles composition varied from about 0.5% in BG sampling to 7.4% on 16 April 2009.

Silicate mixtures mainly consist of silicates internally mixed with different species such as Si-rich, Ca-bearing, metals and biogenic particles. They were identified by means of the EDX spot analysis revealing heterogeneous phases within the single particle. A high content of silicates/S-rich mixtures were observed in the warmer samplings (9% on 31 July and 10.4% on 16 September), whereas, the highest content of silicates-carbonates mixtures was found in BG sampling.

Qualitative Remarks on Fine Fraction

The fine fraction of both BG and polluted samples was essentially constituted of an agglomerate state matter, with crystals re-grown on filters and K as the prevailing element (Fig. 7(a)). The agglomerate state of atmospheric aerosol on finer stages can be explained by the hygroscopic behavior of mixed inorganic and organic aerosol, as studied by Mikhailov *et al.* (2009). In that work authors explain how, due to the effect of relative humidity variation, the mixing of organic and inorganic aerosols could cause the formation of the agglomerate matrix. Mikhailov *et al.* (2009) supposed this effect to be much more evident in cases of multi-component mixtures, characteristic of the mixed atmospheric aerosols state. For this reason the presence of organic and

Table 2. Groups and elemental composition in the coarse fraction for, respectively, BG and polluted samplings of 350 individual particles per day, with corresponding percentages of occurrence.

Particle groups	Major selection criteria Chemical[1], Morphological and Beam Resistence	08/02/2011 BG	18/03/2010 polluted	16/04/2009 polluted	31/07/2008 polluted	16/09/2010 polluted
Silicate	Si + Al > 60%	22.5	24.5	39.8	10.8	12.5
Silicate with sulfur	Silicate + S	0.0	6.9	14.0	4.8	10.4
Ca-bearing	Ca + Mg > 90% sometimes with minor Fe or P	40.1	23.8	9.2	33.1	8.8
Metal oxide/Hydroxide	Metals (Fe, Zn, Al, Mn, Cu, Ti) > 80%	9.6	18.9	8.0	6.6	9.8
S-rich	S > 30% and/or Ca,Mg, K, Na > 40%	0.5	2.7	6.0	9.6	20.7
Soot	Morphology	12.6	2.9	0.9	3.3	2.4
Biogenic	Complex morphology and/or minor elements (P, K, Cl, S), often beam damaged	1.3	3.2	4.3	10.5	14.3
Si-rich	Si > 85%	8.0	5.1	4.6	2.1	3.7
Fly ash	Si + Al > 60% and spherical	0.5	3.2	7.4	6.3	3.0
Silicate mixtures	Mixtures of silicates and other particle groups (Ca-bearing, biogenic, metal oxide/hydroxide)	4.3	2.4	0.6	3.6	4.0
Silicate/S-rich mixtures	Mixtures of silicates and S-rich	0.5	6.4	5.2	9.0	10.4

[1] X-ray intensities of elements relative to the sum of net counts of elements with Z > 10.

Table 3. Silicate classes and their elemental composition in the coarse fraction for, respectively, BG and polluted samplings, with corresponding percentages of occurrence.

SILICATE CLASSES	08/02/11	18/03/10	16/04/09	31/07/08	16/09/10
[1]Si-Al-(Na, Mg, K, Ca, Fe)	12.3	22.7	51.0	13.5	19.7
[2]Si-Ca-Fe	0.1	0.0	0.0	0.9	0.0
[3]Si-Al-(Na-Ca, K)	10.0	8.8	2.8	1.2	3.0

[1] Clay minerals; [2] Ca-Silicates; [3] feldspars.

inorganic mixtures in the agglomerate matrix can be hypothesized for fine filters examined in the present work. The confirmation of this assumption was derived by direct observations of the peripheral zones of the impaction spot where many soot particles and TB were found (Fig. 7(b)).

Re-growth effects observed on the filters impaction spot (Wittmaack *et al.*, 2002) suggest the sampling of soluble aerosol species that gave origin to crystals on the agglomerate matrix. These crystals were typically found as K-, NH_3-, Ca- sulfates and/or nitrates crystal salts (Fig. 7(c)), easily damaged by the electron beam (Vester *et al.*, 2007). A relevant difference between BG and polluted air-masses is that in the first case K usually forms nitrates, whereas in polluted cases K-sulfates prevail.

K-sulfate crystals were mostly prismatic, sometimes rhombohedral, hexagonal or swallow-tail twin (Fig. 7(c)). They were observed on stages 1–8 and the biggest dimensions were found on stage 6 (0.26 μm–0.38 μm), where they reach dimensions up to 250 μm–300 μm.

Moving from smaller to larger dimensions, a change in the S-crystals composition was observed, with K replaced by Ca, giving rise to S-K-Ca and S-Ca phases. S-K-Ca can be considered as a transition phase between S-K and S-Ca crystals. These latter were mainly found in the fraction 0.61 μm–1.58 μm as acicular or hexagonal plate-like aggregate particles (Fig. 7(d)). In addition, S-rich crystals with prismatic, hexagonal and sub-rounded shape and S-Mg-Zn composition (Fig. 7(e)) characterized the fraction 0.26 μm–0.94 μm. These observations show how these secondary phases are grain-size dependent.

Along with crystals re-grown on filters, agglomerate structures with dimensions of a few microns, constituted by Si, Al, S, K, Fe, were common to all samplings (Fig. 7(f)), but much more frequent on 16 April 2009. Despite their dimensions, these structures were unexpectedly found in the ultra-fine stages (EAD < 0.1 μm) with a gel-like aspect, probably derived by de-hydration of the soluble silicate phases (Lee and Van Deventer, 2002). The highest content of fly ash (Table 2) in the coarse fraction of 16 April 2009 could suggest a process of fly-ash leaching (Gitari *et al.*, 2009) that gives rise to soluble silicates observed as gel-like structures on the fine mode. Similar agglomerates with a Si-rich composition (without quartz structure) were observed too.

In addition, transition metals (Fe, Mn, Zn, Cu, Cr, V) were detected in the agglomerate matrix of all samplings. Fe-rich phases were found as a coating of particles, as seen by means of backscattered electron images (Figs. 7(g)–7(h)). Spherical Fe-rich particles were also present as primary oxide (Fig. 7(a)) sometimes together with other metals such as Mn, Cu, Cr, V characterizing mainly BG and 18 March 2010 samplings.

Fly ash and cenospheres were especially found on 16 April 2009.

DISCUSSION AND CONCLUSIONS

Peculiar features observed in the polluted aerosol coarse compositions provided information on their possible sources, both local and trans-boundary. Comparison with BG particle characteristics allows for the understanding of how air mass circulation affects aerosol composition in a South-Italy semi-rural site. Main signatures of BG day are nitrate coated Ca-bearing particles, Si-rich particles and soluble phases of Zn or Fe, sometimes found internally mixed with soot agglomerates (Fig. 8(a)). The metal particles percentage is comparable to values found on other polluted days (16 April, 31 July, 16 September), probably due to local anthropogenic sources.

As well as on BG day, the polluted air mass on 18 March 2010 was characterized by abundant feldspars, in disagreement with local geology and soil composition (official geological cartography of Italy at www.isprambiente.gov.it/Media/carg/470_POTENZA/Foglio.html), thus suggesting local anthropogenic sources (steel plant and bricks production). Similarly to BG sampling, nitrate coated Ca-bearing particles (Fig. 8(b)), Si-rich particles, soluble Fe phases, in coarse fractions, and abundance of K in fine fractions were observed. These components can be traced to both domestic heating (Popovicheva *et al.*, 2015) and the burning of tree branches, in particular olive trees (Demirbas, 2004), which are diffused activities in this area in late winter/early springtime (Dambruoso *et al.*, 2014). Moreover, Ca and Si-rich aerosols are typical emissions of red oak wood burning (Demirbas, 2004), which could have been locally used to heat private houses. Soluble Zn and Fe phases also support domestic heating and biomass burning as contributing sources for BG (8 February 2011) and 18 March 2010, since these elements are important constituents of vegetation (Fu *et al.*, 2012).

On 18 March, both embedded soot and soot agglomerates (Fig. 8(c)) (China *et al.*, 2013; Diapouli *et al.*, 2014) were also found with aluminosilicates rich in Zn, Cu and Mn, fly ash, rich-Fe (Table 5) and gypsum particles inclusions, indicating a long-range transport effect (Fig. 6(e), top panel). All these mixed particles suggest coal power plant (Veranth *et al.*, 2000) and/or waste incinerators as additional pollution sources (Yoo *et al.*, 2002) which could also explain the highest metals contribution, especially spherical and non-spherical Fe-rich and Al-rich particles. Opposite to BG,

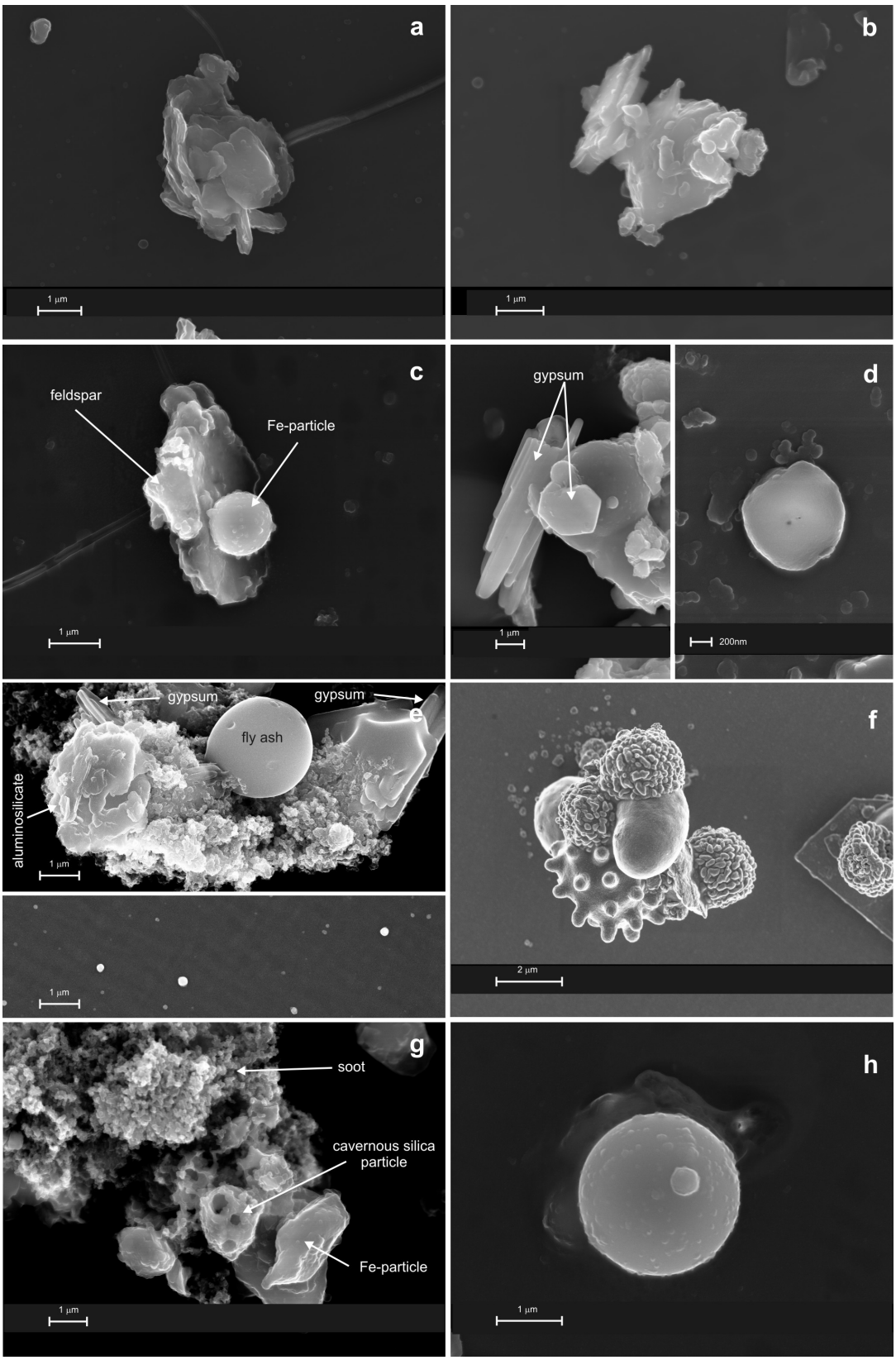

Fig. 6. FESEM images of particles in coarse fraction of both polluted and BG samples. (a) Aggregates of rich - Si, Al, and K flakes; (b) Ca-Mg particle ; (c) Fe-rich spherical particles on feldspar; (d) hexagonal plate and elongated Ca-S shape (left side) and Ca-S with nitrate coating on surface (right side); (e) large agglomerate of soot with inclusions of fly ash, gypsum and aluminosilicate particles (top panel) and tar balls (bottom panel); (f) biogenic particles; (g) Si-rich cavernous particle (cenosphere) with soot and Fe-rich particle; (h) fly ash particle.

Table 4. Ca-bearing classes and their elemental composition in the coarse fraction for, respectively, BG and polluted samplings, with corresponding percentages of occurrence.

CA-BEARING CLASSES	08/02/11	18/03/10	16/04/09	31/07/08	16/09/10
Ca-particles	26.2	6.4	2.0	19.3	3.7
Ca-Mg-particles	13.4	16.3	7.2	13.9	5.2
Ca-Mg-P-particles	0.0	1.1	0.0	0.0	0.0
Ca-Fe--particles	0.5	0.0	0.0	0.0	0.0

Table 5. Metal classes and their elemental composition in the coarse fraction for, respectively, BG and polluted samplings, with corresponding percentages of occurrence.

METAL CLASSES	08/02/11	18/03/10	16/04/09	31/07/08	16/09/10
Fe-rich particles	6	15.5	7.4	3.3	6.9
Zn-rich particles	1.9	0.0	0.0	0.0	0.0
Fe-Zn-rich particles	1.1	1.9	0.6	3.3	2
Al-rich particles	0.6	1.6	0	0	0.9

Table 6. S-rich classes and their elemental composition in the coarse fraction for, respectively, BG and polluted samplings, with corresponding percentages of occurrence.

S-RICH CLASSES	08/02/11	18/03/10	16/04/09	31/07/08	16/09/10
S-(Ca, Mg, K, Na)	0.5	2.7	6.0	3.9	20.7
Ca-rich-sulfate-particles	0.0	0.0	0.0	5.7	0.0

S-reacted particles, namely silicates with S, S-rich particles and silicate/S-rich mixtures, represent a high fraction of total particles, (16% vs. 1%, see Table 2), indicating a S-rich air mass advection that also explains prevailing K-sulfates in the 18 March fine fraction, compared to K-nitrates in BG.

Among the polluted air mass families (Table 2), the highest amount of aluminosilicates particles and fly ash, with a similar composition (Si-Al-Mg-K-Ca-Fe), was found on the 16 April 2009 sampling. In the fine fraction fly ash and/or cenospheres were observed together with gel-like phases that, due to their peculiar composition, provide support for coal power plants in eastern Europe (see Fig. 3(b)) and/or cement plants as possible industrial sources (Gitari *et al.*, 2009). As for 18 March, embedded soot particles, and/or their internally mixing with aluminosilicates, fly ash and gypsum can be explained by particle transformation processes due to long-range transport. A further signature of air mass transport can be highlighted by considering the significant percentage of S-reacted particles (25.2%).

On 31 July 2008, a high content of nitrate coated Ca-bearing particles (Table 6) suggests a contribution from biomass burning, whereas S-rich and fly ash particles indicate industrial sources. As for biomass burning, wildfire events in the Mediterranean area (see Figs. 3 and 4) could also be responsible for the abundant Ca-bearing particles due to the increased soil particles re-suspension effect (Diapouli *et al.*, 2014). As for the industrial contribution, following Del Monte and Sabbioni, 1984, gypsum crystal nucleation on fly ash particles observed for this sampling (Fig. 8(d)), could indicate the emission of fly ash from coal power plant. With regard to the abundance of Ca-rich-sulfate-particles, possible sources such as cement production, surface weathering of limestone and flue-gas desulfurization can be hypothesized (Bigham *et al.*, 2005). Moreover, due to the summer season, biogenic particles represent a relevant percentage for this sampling, if compared to the BG one. As for the other polluted air masses, S abundance is confirmed by a higher amount of S-reacted particles (23.4%) compared to BG conditions (1%) as reported in Table 2.

Air mass pathways crossing a S-rich atmosphere produced, on 16 September 2010, (see Figs. 3 and 4) the highest percentages of both total S-reacted particles (41.5%) and of Ca-S particles (17.7%). The concurrent lowest amount of Ca-bearing particles suggests their depletion due to the high S content that favored the Ca-S particles formation. In this case the anthropogenic signature can be derived by the presence of both spherical and non spherical Fe-particles, along with Ca-bearing particles, Ca-S and fly ash, related to biomass burning and industrial emissions.

Based on these observations, it can be highlighted that different features typify the four polluted air masses apart from seasonal local sources. Advected particles suggest different possible origins depending on the day as such as coal power plant and/or waste incinerators on 18 March, coal power plants and/or cement plants on 16 April, biomass burning, coal power plants and/or cement plants on 31 July, biomass burning and industrial emissions on 16 September. The relevant impact of long-range transport on aerosol properties can be summarized in the following:

- Embedded soot and/or large soot agglomerates internally mixed with silicate particles rich in Cu and Zn, Ca-S, fly ash and metals particles in the coarse fraction of the polluted sampling, can result in an extensive modification of both aerosol size and chemical properties.
- Soot agglomerates can be carriers of heavy metals.
- An abundance of S in polluted air masses favors K-sulfate formation in the fine fractions, which is opposite to the BG condition, when K-nitrates prevail. This variation

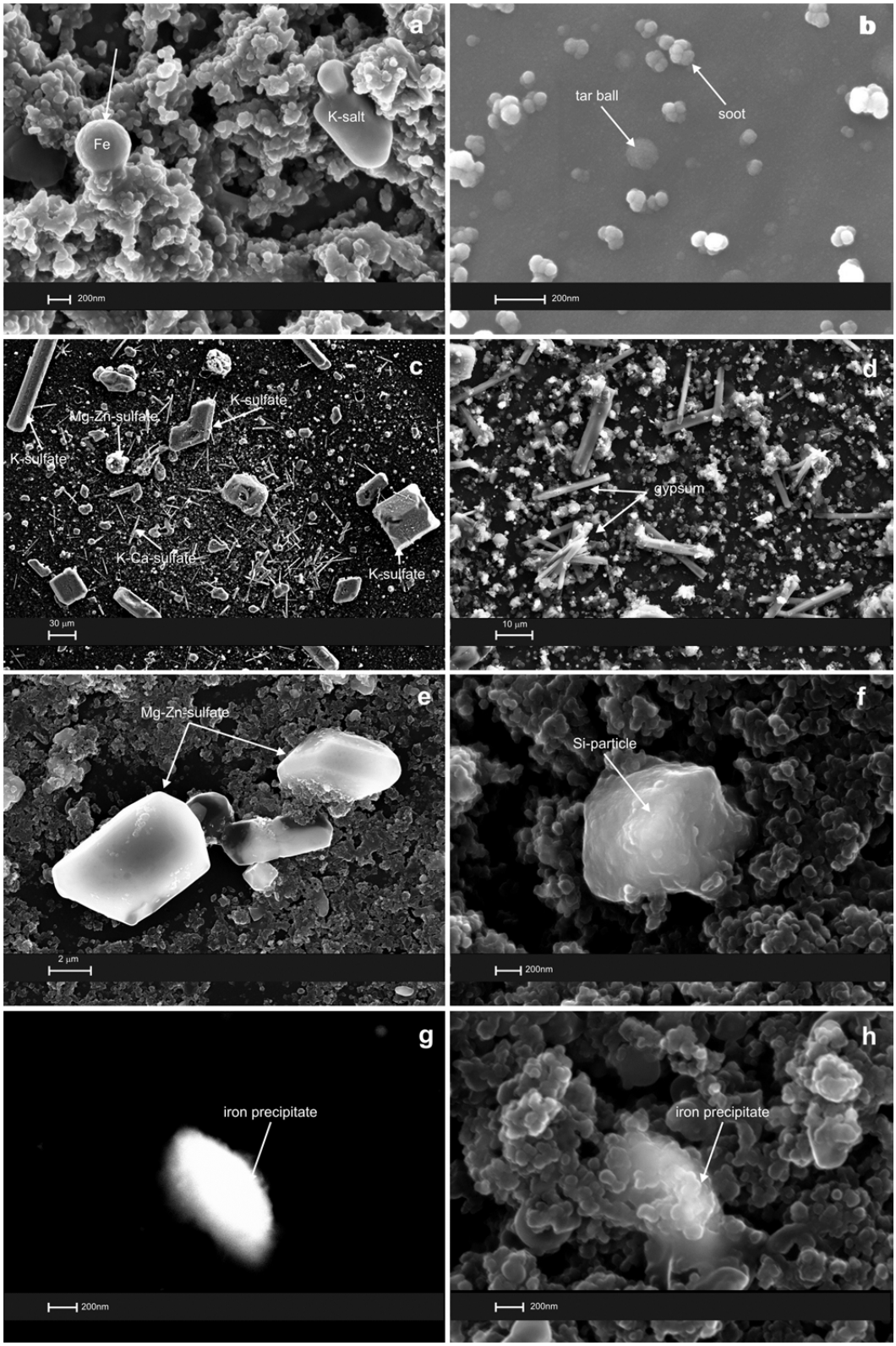

Fig. 7. FESEM images of particles in fine fraction of the polluted and backgrond samples. (a) agglomerate state matter dominating the fine fraction with crystal salts (K-S-sulfates) due to re-growth effect and included particle (Fe-rich spherical); (b) soot and organic aerosols (tar balls); (c) different kinds of sulfates found in stage 7 on polluted samples; (d) elongate and radial aggregate gypsum crystals in stage 8 on both BG and polluted samples; (e) re-growth of large Mg-Zn-sulfate crystals in stage 6 and 7 on both BG and polluted samples; (f) Si-rich particle with gel-like aspect in the ultrafine fraction of both polluted and BG samples; (g) backscattered electron images of Fe-rich phases found as agglomerate state matter coating; (h) same as (7g) with secondary electron detector.

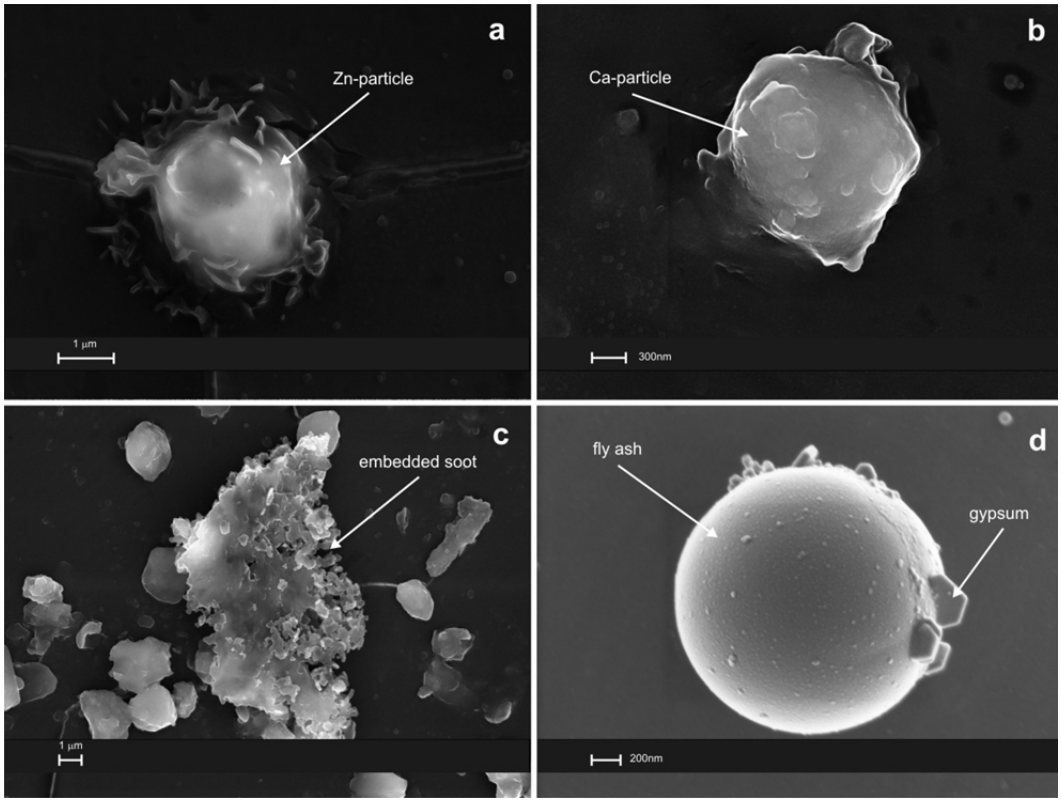

Fig. 8. FESEM images of particles on coarse filters: (a) water soluble Zn specie in BG coarse fraction; (b) Ca-bearing particle with nitrate coating; (c) partially embedded soot particle; (d) fly ash particle with gypsum nucleated on its surface.

could affect atmosphere radiative properties, due to different optical properties of nitrates and sulfates as in Zhang *et al.* (2012).

- Chemical reactions with N- and S- compounds allow Ca-bearing and metal (Fe, Zn, Al) particles to be available in a soluble phase.
- S-reacted particles represent a signature of the influence of anthropogenic activities, even for sites without significant local sources of pollution.

To sum up, the obtained results underline the strong influence of polluted air mass advection over sites without strong emissions sources, modifying air quality and possible health effects. For this reason, reproducing this kind of study in other sites would assess pollution impact on a larger scale and would improve aerosol properties knowledge.

ACKNOWLEDGMENTS

Authors would like to thank the three anonymous referees for their useful comments and suggestions which helped to improve the quality of the paper.

This study was partially financially supported by the Associazione Italiana per lo Studio delle Argille - onlus.

Authors are thankful to the NOAA Air Resources Laboratory (ARL) for HYSPLIT model and READY website (http://www.arl.noaa.gov/ready.php) allowing air mass calculation and to the NRL/Monterey Aerosol Page for NAAPS maps used in this study.

REFERENCES

Adachi, K. and Buseck, P.R. (2010). Hosted and free-floating metal-bearing atmospheric nanoparticles in Mexico City. *Environ. Sci. Technol.* 44: 2299–2304.

Bigham, J.M., Kost, D.A., Stehouwer, R.C., Beeghly, J.H., Fowler, R., Traina, S. J., William E.W. and Dick, W.A. (2005). Mineralogical and engineering characteristics of dry flue gas desulfurization products. *Fuel* 84: 1839–1848.

Bovchaliuk, A., Milinevsky, G., Danylevsky, V., Goloub, P., Dubovik, O., Holdak, A., Ducos, F. and Sosonkin, M. (2013). Variability of aerosol properties over Eastern Europe observed from ground and satellites in the period from 2003 to 2011. *Atmos. Chem. Phys.* 13: 6587–6602.

Caggiano, R., Fiore, S., Lettino, A., Macchiato, M., Sabia, S. and Trippetta, S. (2011). $PM_{2.5}$ measurements in a Mediterranean site: Two typical cases. *Atmos. Res.* 102: 157–166.

Calvello, M., Esposito, F., Pavese, G. and Serio, C. (2010). Physical and optical properties of atmospheric aerosols by in-situ and radiometric measurements. *Atmos. Chem. Phys.* 10: 2195–2208.

Cheng, T., Wu, Y., Gu, X. and Chen, H. (2015). Effects of mixing states on the multiple scattering properties of soot aerosols. *Opt. Express* 23: 10808–10821.

China, S., Mazzoleni, C., Gorkowski, K., Aiken, A.C. and Dubey, M.K. (2013). Morphology and mixing state of individual freshly emitted wildfire carbonaceous particles.

Nat. Commun. 4: 2122.

Dambruoso, P., de Gennaro, G., Di Gilio, A., Palmisani, J. and Tutino, M. (2014). The impact of infield biomass burning on PM levels and its chemical composition. *Environ. Sci. Pollut. Res. Int.* 21: 13175–13185.

Del Monte, M. and Sabbioni, C. (1984). Gypsum crusts and fly-ash particles on carbonatic outcrops. *Arch. Meteorol. Geophys. Bioklimatol. B* 35: 105–111.

Demirbas, A. (2004). Combustion characteristics of different biomass fuels. *Prog. Energy Combust. Sci.* 30: 219–230.

Diapouli, E., Popovicheva, O., Kistler, M., Vratolis, S., Persiantseva, N., Timofeev, M., Kasper-Giebl, A. and Eleftheriadis, K. (2014). Physicochemical characterization of aged biomass burning aerosol after long-range transport to Greece from large scale wildfires in Russia and surrounding regions, Summer 2010. *Atmos. Environ.* 96: 393–404.

Draxler, R.R. and Rolph, G.D. (2003). HYSPLIT (Hybrid Single-Particle Lagrangian Integrated Trajectory) model, http://www.arl.noaa.gov/ready/hysplit4.html, NOAA Air Resour. Lab., Silver Spring, MD.

Esposito, F., Leone, L., Pavese, G., Restieri, R. and Serio, C. (2004). Seasonal variation of aerosols properties in South Italy: A study on aerosol optical depths Ångström turbidity parameters and aerosol size distributions. *Atmos. Environ.* 38: 1605–1614.

Fu, H., Lin, J., Shang, G., Dong, W., Grassian, V.H., Carmichael, G.R., Li, Y. and Chen, J. (2012). Solubility of iron from combustion source particles in acidic media linked to iron speciation. *Environ. Sci. Technol.* 46: 11119–11127.

Geng, H., Hwang, H., Liu, X., Dong, S. and Ro, C.U. (2014). Investigation of aged aerosols in size-resolved Asian dust storm particles transported from Beijing, China, to Incheon, Korea, using low-Z particle EPMA. *Atmos. Chem. Phys.* 14: 3307–3323.

Gitari, W.M., Fatoba, O.O., Petrik, L.F. and Vadapalli, V.R.K. (2009). Leaching characteristics of selected South African fly ashes: Effect of pH on the release of major and trace species. *J. Environ. Sci. Health., Part A* 44: 206–220.

Hochella, M.F., Moore, J.N., Putnis, C.V., Putnis, A., Kasama, T. and Eberl, D.D. (2005). Direct observation of heavy metal-mineral association from the Clark Fork River Superfund Complex: Implications for metal transport and bioavailability. *Geochim. Cosmochim. Acta* 69: 1651–1663.

IPCC: Intergovernmental Panel on Climate Change, Climate Change 2013: The Physical Science Basis: Working Group I Contribution to the Fifth Assessment Report of the Intergovernmental Panel on Climate Change, Cambridge University Press: New York, USA, 2013.

Janssen, N.A., Hoek, G., Simic-Lawson, M., Fischer, P., van Bree, L., ten Brink, H., Keuken, M., Atkinson, R.W., Anderson, H.R., Brunekreef, B. and Cassee, F.R. (2011). Black Carbon as an Additional Indicator of the Adverse Health Effects of Airborne Particles Compared with PM_{10} and $PM_{2.5}$. *Environ. Health Perspect.* 119: 1691–1699.

Jouan, C., Pelon, J., Girard, E., Ancellet, G., Blanchet, J.P. and Delanoë, J. (2014). On the relationship between Arctic ice clouds and polluted air masses over the North Slope of Alaska in April 2008. *Atmos. Chem. Phys.* 14: 1205–1224.

Lee, W.K.W. and Van Deventer, J.S.J. (2002). Structural reorganisation of class F fly ash in alkaline silicate solutions. *Colloids Surf. A* 211: 49–66.

Lettino A. and Fiore S. (2013). Provenance of inorganic aerosol using single-particle analysis: A case study. *Sci. Total Environ.* 463–464: 404–413.

Li, W.J. and Shao, L Y. (2009a). Observation of nitrate coatings on atmospheric mineral dust particles. *Atmos. Chem. Phys.* 9: 1863–1871.

Li, W. and Shao, L. (2009b). Transmission electron microscopy study of aerosol particles from the brown hazes in northern China. *J. Geophys. Res.* 114: D09302.

Li, W., Shao, L., Zhang, D., Ro, C.U., Hu, M., Bi, X., Geng, H., Matsuki, A., Niu, H. and Chen, J. (2016). A review of single aerosol particle studies in the atmosphere of East Asia: Morphology, mixing state, source, and heterogeneous reactions. *J. Cleaner Prod.* 112: 1330–1349.

Mikhailov, E., Vlasenko, S., Martin, S.T., Koop, T. and Pöschl, U. (2009). Amorphous and crystalline aerosol particles interacting with water vapor: Conceptual framework and experimental evidence for restructuring, phase transitions and kinetic limitations. *Atmos. Chem. Phys.* 9: 9491–9522

Moffet, R.C., Rödel, T.C., Kelly, S.T., Yu, X.Y., Carroll, G.T., Fast, J., Zaveri, R.A., Laskin, A. and Gilles, M.K. (2013). Spectro-microscopic measurements of carbonaceous aerosol aging in Central California. *Atmos. Chem. Phys.* 13: 10445–10459.

Molina, R.M., Schaider, L.A., Donaghey, T.C., Shine, J.P. and Brain, J.D. (2013). Mineralogy affects geoavailability, bioaccessibility and bioavailability of zinc. *Environ. Pollut.* 182: 217–224.

Pardo, M., Porat, Z., Rudich, A., Schauer, J.J. and Rudich, Y. (2016). Repeated exposures to roadside particulate matter extracts suppresses pulmonary defense mechanisms, resulting in lipid and protein oxidative damage. *Environ. Pollut.* 210: 227–237.

Pavese, G., Lettino, A., Calvello, M., Esposito, F. and Fiore, S. (2016). Aerosol composition and properties variation at the ground and over the column under different air masses advection in South Italy. *Environ. Sci. Pollut. Res.* 23: 6546–6562.

Popovicheva, O., Kistler, M., Kireeva, E., Persiantseva, N., Timofeev, M., Kopeikin, V. and Kasper-Giebl, A. (2014). Physicochemical characterization of smoke aerosol du ring large-scale wildfires: Extreme event of August 2010 in Moscow. *Atmos. Environ.* 96: 405–414.

Popovicheva, O.B., Kozlov, V.S., Engling, G., Diapouli, E., Persiantseva, N.M., Timofeev, M.A., Fan, T.S., Saraga, D. and Eleftheriadis, K. (2015). small-scale study of siberian biomass burning: I. smoke microstructure. *Aerosol Air Qual. Res.* 15: 117–128.

Posfai, M., Gelencser, A., Simonics, R., Arato, K., Li, J., Hobbs, P.V. and Buseck, P.R. (2004). Atmospheric tar

balls: Particles from biomass and biofuel burning. *J. Geophys. Res.* 2004: D06213.

Tobo, Y., Zhang, D., Matsuki, A. and Iwasaka, Y. (2010). Asian dust particles converted into aqueous droplets under remote marine atmospheric conditions. *Proc. Natl. Acad. Sci. U.S.A.* 107: 17905–17910.

Veranth, J.M., Fletcher, T.H., Pershing, D.W. and Sarofim, A.F. (2000). Measurement of soot and char in pulverized coal fly ash. *Fuel* 79: 1067–1075.

Vester, B.P., Ebert, M., Barnert, E.B., Schneider, J., Kandler, K., Schutz, L. and Weinbruch, S. (2007). Composition and mixing state of the urban BG aerosol in the Rhein-Main area (Germany). *Atmos. Environ.* 41: 6102–6115.

Wittmaack, K., Menzel, N., Wehnes, H. and Heinzmann, U. (2002). Phase separation and re-growth of aerosol matter collected after size fractionation in an impactor. *Atmos. Environ.* 36: 5877–5886.

Yoo, J.I., Kim, K.H., Jang, H.N., Seo, Y.C., Seok, K.S., Hong, J.H. and Jang, M. (2002). Emission characteristics of particulate matter and heavy metals from small incinerators and boilers. *Atmos. Environ.* 36: 5057–5066.

Zhang, H., Shen, Z., Wei, X., Zhang, M. and Li, Z. (2012). Comparison of optical properties of nitrate and sulfate aerosol and the direct radiative forcing due to nitrate in China. *Atmos. Res.* 113: 113–125.

Received for review, May 30, 2016
Revised, September 8, 2016
Accepted, October 10, 2016